Finite-gain-current repetitive controller for synchronverters with harmonic-sharing capabilities

Róldan-Pérez, J.; Prodanovic, M.; Rodriguez-Cabero, A.; Guerrero, Josep M.; Garcia-Cerrada, A.

Published in:
Proceedings of the ICHQP 2018 - 18th International Conference on Harmonics and Quality of Power

DOI (link to publication from Publisher):
10.1109/ICHQP.2018.8378881

Publication date:
2018

Document Version
Publisher's PDF, also known as Version of record

Finite-Gain-Current Repetitive Controller for Synchronverters with Harmonic-Sharing Capabilities

J. Roldán-Pérez*, M. Prodanovic*, A. Rodríguez-Cabero*, J.M. Guerrero†, and A. García-Cerrada‡
*IMDEA Energy Institute, Madrid, Spain. E-mail: javier.roldan@imdea.org
†Department of Energy Technology, Aalborg University, Aalborg 9220, Denmark.
‡ICAI School of Engineering, Comillas Pontifical University, Madrid, Spain.

***Abstract*—Power electronics interfaces are commonly used for renewable energy integration in microgrids and their control as synchronverters represents an alternative to typical control configurations. This control technique introduces many advantages, but several issues need to be properly addressed including power quality and harmonic current sharing. In this paper, a method to deal with the current harmonics distribution in microgrids based on synchronverters is introduced. A Finite-Gain Repetitive Controller (FRC) is added to the control system of a current-controlled synchronverter. It is shown that the use of this alternative controller allows current harmonics to be shared between the Ditributed Generators (DGs) feeding a non-linear load. In addition, it is shown that the FRC represents a robust solution against the frequency variations typically occurring in microgrids. All the harmonic sharing improvements of the control system are tested on a prototype microgrid consisting of two 15 kVA synchronverters and a non-linear load connected via electrical distribution lines.**

I. Introduction

In recent years, renewable energies have drawn much attention and microgrids are an adequate solution to integrate these energy resources to electrical grids. Commonly, renewable energy sources are connected to microgrids by using droop-controlled power electronics converters [1]. Droop control has become very popular and it has been studied in depth in the literature [2]. However, an alternative way to integrate converters to microgrids is to emulate the dynamics of a synchronous machine and this control strategy is commonly known in the literature as Virtual Synchronous Machines (VSMs) [3], Virtual Synchronous Generators (VSGs) [4], or synchronverters [5]. The emulation of synchronous machines has many potential advantages, but it requires more research effort in order to solve implementation issues like voltage and current limitation [6], the operation under severe voltage disturbances [7], and under distorted grid conditions [8].

Power quality in microgrids has attracted attention of researchers because most electric loads consume non-sinusoidal currents that should be shared between Distributed Generators (DGs) [9]. However, in practical applications the output impedances of DGs are not equal and the loads are connected via distribution lines. These facts make it difficult to distribute harmonic currents properly [10]. The virtual impedance is a control technique that is commonly applied to DGs to address power quality issues and it has been thoroughly studied for droop-controlled Voltage Source Converters (VSCs) [10, 11]. This control technique has been recently applied to improve the output-current quality in parallell-connected VSMs [12]. Most authors apply resistive virtual impedances [13], although some of them apply more advanced control techniques like resonant controllers [12]. An alternative to virtual impedances is a secondary controller that sends harmonic references to the DGs through a communication link. This alternative can be used to improve the current harmonic distribution [14] or the voltage quality in the nodes of a microgrid [15]. However, fast communication links are required [14].

Repetitive controllers (RCs) are popular in power electronics applications such as active power filters [16]. This type of controller provides accurate tracking of periodic signals and its design is quite simple [16]. However, RCs are sensitive to changes in the grid frequency and microgrids are prone to transient frequency variations. Therefore, their application in a microgrid is not straightforward. Several solutions have been proposed in the literature to solve the frequency deviation problem. Some of them are based on adaptive filters that emulate fractional delays [17, 18]. For example, in [19] a Padé filter is proposed to implement the fractional part of the delay that cannot be directly discretized when a RC is implemented. Additionally, Escobar *el al.* [20] propose a fractional delay approximation for a $6k \pm 1$ RC, with succesful results. Similar solutions have been proposed in literature with different degrees of complexity and performance [21–23].

In this paper, a Finite-Gain RC (FRC) is proposed to adjust the output impedance of synchronverters in microgrids in order to control the sharing of current harmonics between them. A current-controlled version of the synchronverter is used to make it possible to apply the FRC. Also, it is demonstrated that a current-controlled synchronverter with a FRC is similar to a classical synchronverter with a harmonic virtual impedance. It is shown that a FRC provides adjustable gain at the harmonic frequencies with an improved performance against frequency variations. All the control system improvements are tested in a microgrid prototype that consists of two 15 kVA synchronverters feeding a non-linear load via electrical distribution lines.

II. Application and Control System Overview

A. System Description and Control Structure

Fig. 1 shows the schematics of a synchronverter-based microgrid. Each VSC is connected to the microgrid via a LCL filter and emulates the dynamics of a synchronous machine.

978-1-5386-0517-2/18/$31.00

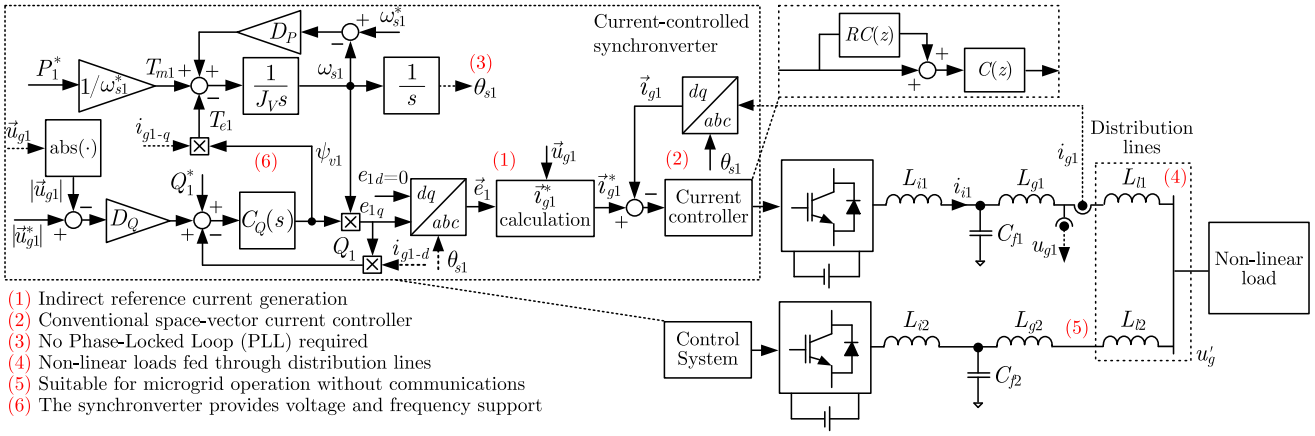

Fig. 1. Control and circuit diagram of a synchronverter based microgrid with non-linear loads. The synchronverters include a current controller, where the FRC is applied. The current controller consists of a main and a harmonic controller, called $C(z)$ and $RC(z)$, respectively.

The virtual machine generates a voltage reference ($\vec{e}$) that is transformed to a current reference ($\vec{i}_g^*$) which is then followed by an internal current controller. The current controller is divided into a main and a harmonic controller. The main controller is called $C(z)$ and provides a fast transient response, while the harmonic controller is called $RC(z)$ and deals with power quality issues. In this paper, it will be shown that a harmonic controller based on a FRC is similar to a harmonic virtual impedance and this is a contribution of this paper. Variables related to a specific DG are noted with the DG number in the subscript (e.g. i_{g1}), but this number will be omitted in the rest of the paper when not necessary.

B. Synchronverter in a Synchronous Reference Frame (SRF)

This section summarizes the synchronverter formulation in a SRF [8].

The synchronverter virtual inertia is given by

$$J_V \cdot d\omega_s/dt = T_m - T_e + D_T(\omega_s^* - \omega_s),\ d\theta_s/dt = \omega_s, \quad (1)$$

where θ_s is the virtual shaft angle, while ω_s and ω_s^* are the synchronous frequency and its reference value, respectively. The virtual inertia is J_V, D_T is the active-power (torque) droop coefficient, while the motion (T_m) and electromagnetic (T_e) torques are defined as

$$T_e = P/\omega_s = \psi_v i_{i-q},\ \ T_m = P^*/\omega_s \approx P^*/\omega_s^*, \quad (2)$$

where $\omega_s \approx \omega_s^*$ in steady state. The injected active power is P and P^* is its set-point value. The synchronverter is synchronized with the q-axis of the VSC output voltage. Therefore, $\vec{e} = e_d + je_q$, with $e_q = \psi_v\omega_s$ and $e_d = 0$, where ψ_v is called "virtual flux" to highlight its similarity with the flux through the permanent magnets of a synchronous machine. This flux is used to control the reactive-power injection:

$$\psi_v = K_Q \int (Q^* + Q_D^* - Q)\, dt, \quad (3)$$

where Q^* is the reactive power set-point and K_Q is the controller gain. The grid voltage support is adjusted with a droop coefficient (D_Q) and the following control law

$$Q_D^* = D_Q(|\vec{u}_g^*| - |\vec{u}_g|), \quad (4)$$

where $|\vec{u}_g|$ is the grid voltage module and $|\vec{u}_g^*|$ is its set point. The active and reactive powers are calculated with [8]:

$$P = \omega_s\psi_v i_{i-q} \approx u_{g-d}i_{g-d} + u_{g-q}i_{g-q}, \quad (5)$$

$$Q = \omega_s\psi_v i_{i-d} \approx u_{g-q}i_{g-d} - u_{g-d}i_{g-q}, \quad (6)$$

where the dq components of the signals involved are calculated with the power-invariant Park's Transformation [24].

C. Current-Controlled Synchronverter

An indirect current controller for a synchronverter was proposed in [25], and it it is used here to simplify the implementation of the FRC. The main idea can be spelled out as follows.

First, by neglecting the filtering capacitor, the synchronverter steady-state equations are:

$$\begin{bmatrix} e_d - u_{g-d} \\ e_q - u_{g-q} \end{bmatrix} = \begin{bmatrix} R_{ig} & -\omega_s L_{ig} \\ \omega_s L_{ig} & R_{ig} \end{bmatrix} \begin{bmatrix} i_{g-d} \\ i_{g-q} \end{bmatrix}, \quad (7)$$

where $L_{ig} = L_i + L_g$ and $R_{ig} = R_i + R_g$. This equation can be used to generate a fictitious current reference ($\vec{i}_g^*$) that is calculated as follows

$$\begin{bmatrix} i_{g-d}^* \\ i_{g-q}^* \end{bmatrix} = K_z \begin{bmatrix} R_{ig} & \omega_s^* L_{ig} \\ -\omega_s^* L_{ig} & R_{ig} \end{bmatrix} \begin{bmatrix} e_d - u_{g-d}^f \\ e_q - u_{g-q}^f \end{bmatrix}, \quad (8)$$

with

$$K_z = 1/(R_{ig}^2 + L_{ig}^2\omega_s^{*2}), \quad (9)$$

where $\vec{u}_g^f$ is a filtered version of $\vec{u}_g$. The block diagram of this control strategy is depicted in Fig. 1, point (1).

D. Current Harmonics in Microgrids

The current harmonic distribution in a microgrid can be studied with the equivalent circuit depicted in Fig. 2, where $G_L(z)$ is the equivalent load admittance and z is the discrete-time Laplace variable. The value of $Z_1(z)$ and $Z_2(z)$ includes

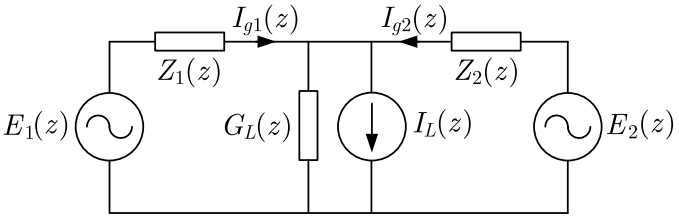

Fig. 2. Electrical circuit used to study harmonic distribution in microgrids.

the DGs electrical and control systems. The ratio between each DG output current and the load current is

$$\frac{I_{g1}(z)}{I_L(z)} = \frac{1/Z_1(z)}{1/Z_1(z) + 1/Z_2(z) + G_L(z)} \tag{10}$$

and

$$\frac{I_{g2}(z)}{I_L(z)} = \frac{1/Z_2(z)}{1/Z_1(z) + 1/Z_2(z) + G_L(z)}. \tag{11}$$

If the DGs have the same rated power, the following relationship can be written

$$R(z) = I_{g1}(z)/I_{g2}(z) = Z_2(z)/Z_1(z), \tag{12}$$

where $R(z)$ will be called "harmonic-sharing ratio".

The discrete-time frequency at the harmonic h is defined as

$$\hat{\omega}_h = e^{j\omega_s h t_s}, \tag{13}$$

where t_s is the sampling period. Along the paper, $\hat{\omega}_h^o$ refers to (13) calculated at the nominal frequency. A value of $|R(\hat{\omega}_h)|$ close to 1 leads to an equal distribution of harmonic currents. If $|R(\hat{\omega}_h)|$ is larger than 1, the DG1 is absorbing a higher percentage of the harmonic current h (and vice-versa if $|R(\hat{\omega}_h)|$ is smaller than 1).

E. Virtual Impedance for Synchronverters

Virtual impedances are commonly used to actively modify the output impedance of DGs. This modification is mainly applied to improve the power-flow control [13], but it can be also used to modify the current harmonic distribution (see (12)) and this is the case studied in this paper [12].

Fig. 3 (a) shows the virtual impedance concept proposed for synchronverters in [12], which can be represented as follows

$$U_i(z) = E(z) - Z_v(z) I_g(z) = E(z) - Z_v(z) P(z) U_i(z), \tag{14}$$

where $E(z)$, $U_i(z)$, and $I_g(z)$ are the discrete-time Laplace transformations of $e(t)$, $u_i(t)$, and $i_g(t)$, respectively. Meanshile, $P(z) = I_g(z)/U_i(z)$ is the plant transfer function and $Z_v(z)$ is the virtual impedance.

III. Proposed Controller Configuration

In this paper, a RC with a non-infinite gain is proposed as an alternative to resonant controllers [12]. However, the use of a RC poses an important problem because it has considerable gain at the fundamental frequency and this can generate an interaction with the virtual synchronous machine. To solve this problem, the indirect current controller explained in Section II-C is applied [25]. Within the current controller,

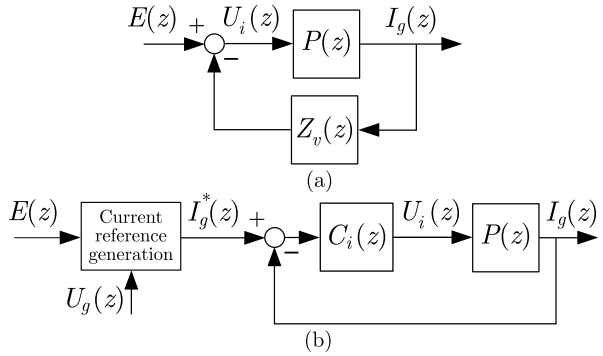

Fig. 3. Control diagram of a synchronverter with (a) a harmonic virtual impedance and (b) an indirect current controller.

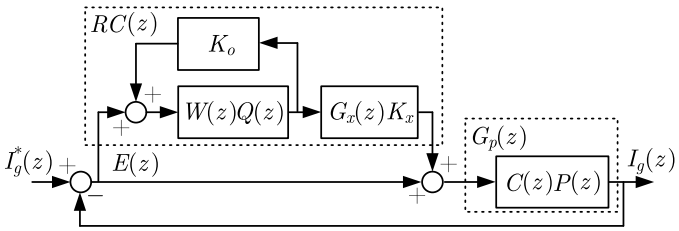

Fig. 4. Block diagram of a Finite-Gain Repetitive Controller (FRC).

the high gain provided by the RC at the fundamental frequency is not a problem. However, the virtual impedance concept cannot be directly applied since the controlled variable is i_g. In order to address this issue, Fig. 3 (a) shows the equivalent control diagram used to design the virtual impedances in [12], while Fig. 3 (b) shows the control diagram of an indirect current controller like in [25]. The open-loop transfer function for the case (a) is

$$G(z) = Z_v(z) P(z), \tag{15}$$

while for the case (b) is (see Fig. 4)

$$G(z) = C_i(z) P(z) = C(z)(1 + RC(z)) P(z). \tag{16}$$

Without loss of generality, the references for each of the control strategies can be written as

$$E(z) = \tilde{E}(z) + \bar{E}(z) \;\text{ and }\; I_g^*(z) = \tilde{I}_g^*(z) + \bar{I}_g^*(z), \tag{17}$$

where the tilde " ˜ " refers to the harmonic components and the bar " ¯ " refers to the fundamental component. If notch filters at the harmonic frequencies are used in the synchronverter [12], it can be guaranteed that $\tilde{E}(z) = 0$ for the case (a), and $\tilde{I}_g^*(z) = 0$ for the case (b). Under this situation, any disturbance-to-output transfer function calculated with (a) or (b) have the same structure. By comparing (15) and (16), the equivalent virtual impedance for the case (b) is

$$Z_v^{eq}(z) = (1 + RC(z)) \cdot C(z). \tag{18}$$

Therefore, the equivalent virtual impedance can be modified by changing the amplification of $RC(z)$ and $C(z)$ at the harmonic frequencies. The design and analysis of a FRC with

this purpose is addressed in detail here and it is the main contribution of this paper.

IV. Finite-Gain Repetitive Controller (FRC)

A. Discrete-Time Finite-Gain Repetitive Controller

The proposed controller is depicted in Fig. 4, where $RC(z)$ is the discrete-time FRC, $G_p(z) = C(z)P(z)$ is the open-loop plant, and $Q(z)$ is a filter that limits the bandwidth. The transfer function $G_x(z)$ and the gain K_x are used to guarantee closed-loop stability. Meanwhile, the gain K_o is used to adjust the FRC amplification at the harmonic frequencies. In order to track even harmonics (only):

$$W(z) = z^{-N/2}, \tag{19}$$

where

$$N/2 = t_s/(t_p/2) \in \mathbb{N}, \tag{20}$$

while t_s and t_p are the sampling and disturbance periods, respectively. Under nominal conditions, $t_p = 1/(2\pi\omega_s^o)$, where ω_s^o is the nominal grid frequency. The transfer function of the proposed FRC is

$$RC(z) = \frac{W(z)Q(z)}{1 - K_o W(z)Q(z)} G_x(z) K_x. \tag{21}$$

B. FRC Stability Analysis

From Fig. 4, the reference-to-error transfer function is:

$$F_e(z) = \frac{1}{1 + G_p(z)} \overbrace{\frac{1 - K_o W(z)Q(z)}{1 - W(z)Q(z)(K_o - K_x G_x(z) F_p(z))}}^{S(z)}. \tag{22}$$

where $F_p(z) = G_p(z)/(1 + G_p(z))$.

A sufficient condition to guarantee closed-loop stability can obtained by applying the small-gain theorem to the system in (22) [26], yielding

$$||W(z)Q(z)(K_o - K_x G_x(z) F_p(z))||_\infty < 1, \tag{23}$$

with $z = e^{j\omega t_s}$. The transfer function $G_x(z)$ is commonly chosen as $\hat{F}_p^{-1}(z)$ in order to maximize stability margins, where $\hat{F}_p(z)$ is a model of $F_p(z)$ [16]. Also, $|Q(e^{j\omega t_s})| \approx 1$ within the RC bandwidth, while $|Q(e^{j\omega t_s})| \approx 0$ out of it. In this case, the stability condition in (23) is reduced to

$$|K_o - K_x| < 1, \tag{24}$$

which is valid for any configuration of $W(z)$ provided that $|W(e^{j\omega t_s})| \leq 1\ \forall\omega$. The value of K_o will be set to fulfil the bandwidth requirements. Therefore, the maximum value of K_x that leads to a stable system can be obtained by solving (24), yielding

$$0 < K_x < 1 + K_o, \tag{25}$$

if $K_o > 0$. It can be seen that the smaller K_o is, the smaller the maximum value of K_x becomes.

C. Equivalent Virtual Impedance

The equivalent harmonic virtual impedance value can be obtained by substituting $z = \hat{\omega}_h$ in $Z_v^{eq}(z)$ (see (18)), yielding

$$R_h = |Z_v^{eq}(\hat{\omega}_h)| = \frac{1 - K_o + K_x}{1 - K_o} \cdot |C(\hat{\omega}_h)| \cdot |G_x(\hat{\omega}_h)|. \tag{26}$$

The value of R_h can be chosen by modifying either K_o or K_x. However, it also depends on $|C(\hat{\omega}_h)|$ and $|G_x(\hat{\omega}_h)|$. The value of K_o will be chosen according to the bandwidth requirements, as will be explained in Section VI-B. Meanwhile, R_h will be set according to the harmonic sharing needs. Therefore, the value of K_x is fixed and it can be calculated as follows

$$K_x = (1 - K_o)R_h'/(|C(\hat{\omega}_{h'})| \cdot |G_x(\hat{\omega}_{h'})|) - 1 + K_o, \tag{27}$$

where h' is one of the harmonic frequencies. From (27), it is clear that the virtual impedance can be set, exactly, only for the harmonic h'. Also, K_x must comply with the stability condition in (25). If this does not occurs, either R_h or K_o (preferably) can be modified.

V. Case Study and System Description

The DG1 is connected to the microgrid via an *LCL* filter whose parameters are $L_i = 2.3$ mH, $C_f = 8.8$ μF, and $L_g = 0.9$ mH. In this case study, the DG1 is connected close to the load, so L_{g1} and R_{g1} are zero. The VSC2 has the same *LCL* filter, but the line impedance is $L_{g2} = 5$ mH and $R_{g2} = 0.2$ Ω. The DC-link voltage of both converters is maintained constant at 680 V with a diode rectifier and a step-up transformer connected to an auxiliary grid. The total DC-link capacitance is 2 mF.

The switching and sampling frequencies are configurable, and they have been set to 10 kHz. The dead-time of both VSCs is 2 μs. The min-max method is used to generate the Pulse Width Modulation (PWM) signal [27]. The non-linear load is a diode-rectifier with a configurable active DC load.

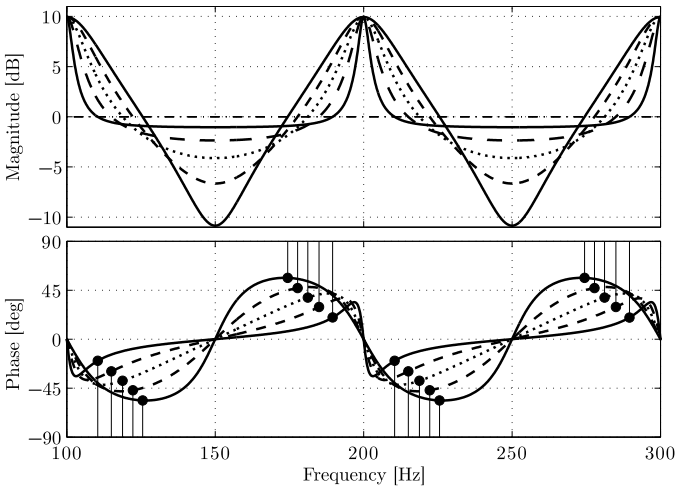

Fig. 5. Bode diagram of $1 + RC(z)$, for K_o =0.5, 0.6, 0.7, 0.8, and 0.9. $R_h = 10$ dB. The black dots are phase margins.

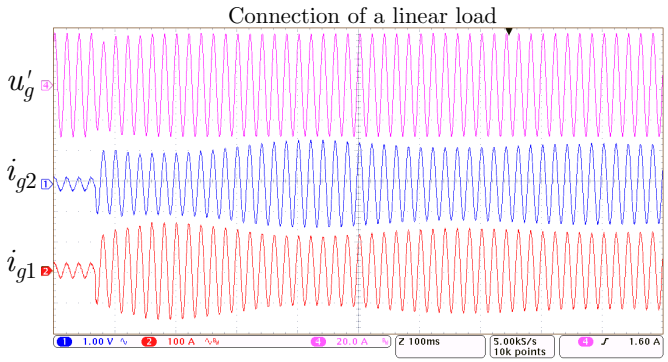

Fig. 6. Operation of the synchronverter-based microgrid feeding a linear load.

VI. Control System Design

A. Main and Harmonic Controller Parameters

The value of N calculated with (20) is 100. The RC bandwidth has been set to 1900 Hz with a 25th-order linear phase FIR filter. The possible values of K_o will be explored in the next section, while K_x will be set according to (27). The RC is implemented as suggested in [19]. The current controller $C(z)$ is a classical PI controller designed with a phase margin of 65 deg and a crossover frequency of 200 Hz. The classical decoupling equations are used [27]. The discrete-time version of the continuous-time plant transfer-function $(P_c(s))$ is obtained with the ZOH method [28].

B. Design of the Gain K_o

Fig. 5 shows the frequency response of $1+RC(z)$ when the value of K_o is modified and K_x is adjusted so that the virtual resistance (R_h) is 10 dB, while the value of K_x is set with (27) (see (26)). It can be seen that the lower the value of K_o, the more robust the system becomes against frequency variations. However, the stability margins are deteriorated (because K_x is closer to its limits). For the application, the value of K_o has been adjusted so that the current harmonics are correctly distributed between the DGs.

VII. Experimental Results

A. Operation with a Linear Load

Fig. 6 shows the operation of the synchronverter-based microgrid feeding a load that consumes active power. Initially, the load was consuming 1 kW. Eventually, an 8 kW load was connected to the microgrid. At his time, a transient in the grid voltage took place. When this transient ended, the current was correctly shared between the DGs because the droop coefficients of both VSCs were the same.

B. Finite-Gain RC to Improve the Harmonic Sharing

Fig. 7 shows the output current of the synchronverters (a) before and (b) after turning on the FRC. When the FRCs are not included the harmonic distribution between the DGs is not adequate. When the FRCs were applied, as shown in Fig. 7 (b), the harmonic sharing between the DGs was controlled and the waveforms became similar. However, the quality of the grid voltage worsened.

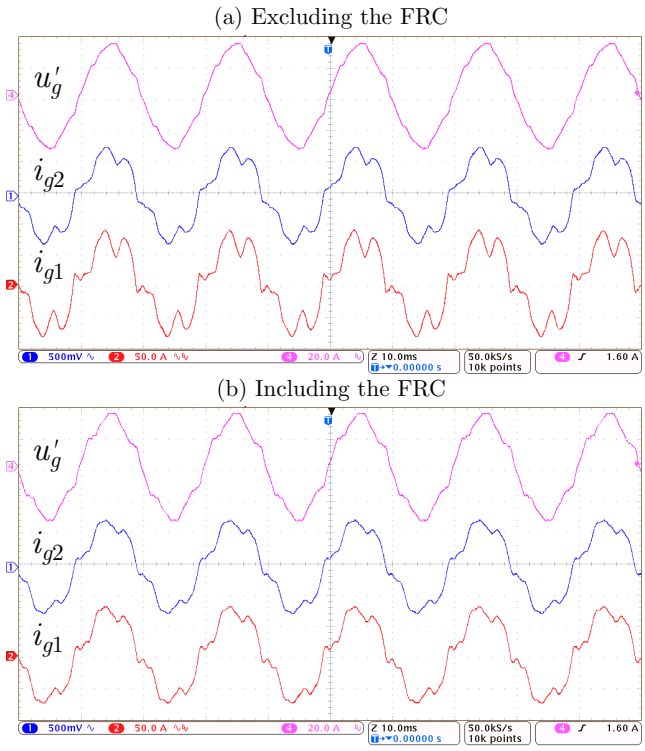

Fig. 7. Operation of the synchronverter-based microgrid (a) excluding and (b) including the FRC.

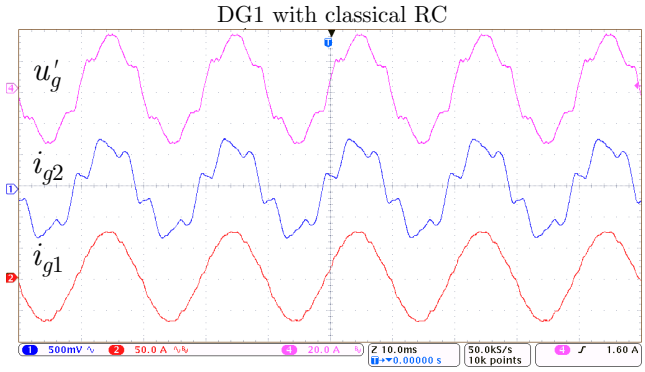

Fig. 8. Operation of the synchronverter-based microgrid feeding a linear load. A classical RC ($K_o = 1$) is applied to the DG1.

C. Infinite Gain Repetitive Controller

Fig. 8 shows the microgrid operation when a classical RC ($K_o = 1$) was applied to the DG1. It can be seen that the quality of output current improved. However, the quality of the grid voltage worsened and all the harmonics were delivered to the load by the DG2. This situation is undesiderable and it should be avoided.

VIII. Conclusion

This paper has shown the application of a Finite-Gain Repetitive Controller (FRC) to the current harmonic distribution improvement in a synchronverter-based microgrid. Firstly, the similarities between a current-controlled and a

classical synchronverter with a virtual impedance have been highlighted. Secondly, it has been shown that the FRC greatly improves the bandwidth when infinite gains at resonance frequencies are not required. The results have demonstrated that the harmonic sharing ratio can be close to one, even thought the FRC is accurately applied only to a single harmonic frequency. All the proposed control system improvements have been tested in a prototype of two synchronverters feeding a non-linear load.

ACKNOWLEDGEMENTS

This work has received financial support by the Community of Madrid Government, Spain, through the research project PRICAM (S2013/ICE-2933)

REFERENCES

[1] J. Guerrero, M. Chandorkar, T. Lee, and P. Loh, "Advanced control architectures for intelligent microgrids-Part I: decentralized and hierarchical control," *IEEE Transactions on Industrial Electronics*, vol. 60, no. 4, pp. 1254–1262, April 2013.

[2] Q. C. Zhong, "Power-electronics-enabled autonomous power systems: Architecture and technical routes," *IEEE Transactions on Industrial Electronics*, vol. 64, no. 7, pp. 5907–5918, July 2017.

[3] S. D'Arco and J. A. Suul, "Equivalence of virtual synchronous machines and frequency-droops for converter-based microgrids," *IEEE Transactions on Smart Grid*, vol. 5, no. 1, pp. 394–395, Jan 2014.

[4] H. Wu, X. Ruan, D. Yang, X. Chen, W. Zhao, Z. Lv, and Q. C. Zhong, "Small-signal modeling and parameters design for virtual synchronous generators," *IEEE Transactions on Industrial Electronics*, vol. 63, no. 7, pp. 4292–4303, July 2016.

[5] Q. C. Zhong and G. Weiss, "Synchronverters: Inverters that mimic synchronous generators," *IEEE Transactions on Industrial Electronics*, vol. 58, no. 4, pp. 1259–1267, April 2011.

[6] O. Mo, S. D'Arco, and J. A. Suul, "Evaluation of virtual synchronous machines with dynamic or quasi-stationary machine models," *IEEE Transactions on Industrial Electronics*, vol. PP, no. 99, pp. 1–1, 2016.

[7] Z. Shuai, W. Huang, C. Shen, J. Ge, and Z. J. Shen, "Characteristics and restraining method of fast transient inrush fault currents in synchronverters," *IEEE Trans. on Ind. Elec.*, vol. 64, no. 9, pp. 7487–7497, Sept 2017.

[8] J. Roldán-Pérez, M. Prodanovic, and A. Rodríguez-Cabero, "Detailed discrete-time implementation of a battery-supported synchronverter for weak grids," in *43nd Annual Conference of the IEEE Industrial Electronics Society (IECON)*, 2017.

[9] J. He, Y. W. Li, F. Blaabjerg, and X. Wang, "Active harmonic filtering using current-controlled, grid-connected dg units with closed-loop power control," *IEEE Trans. on Pow. Elec.*, vol. 29, no. 2, pp. 642–653, Feb 2014.

[10] J. He, Y. W. Li, J. Guerrero, F. Blaabjerg, and J. Vasquez, "An islanding microgrid power sharing approach using enhanced virtual impedance control scheme," *IEEE Transactions on Power Electronics*, vol. 28, no. 11, pp. 5272–5282, Nov 2013.

[11] J. He and Y. W. Li, "Analysis, design, and implementation of virtual impedance for power electronics interfaced distributed generation," *IEEE Trans. on Industry App.*, vol. 47, no. 6, pp. 2525–2538, Nov 2011.

[12] J. Roldán-Pérez, A. Rodríguez-Cabero, and M. Prodanovic, "Harmonic virtual impedance design for a synchronverter-based battery interface converter," in *6th International Conference on Renewable Energy Research and Applications*, November 2017.

[13] W. Yao, M. Chen, J. Matas, J. M. Guerrero, and Z. M. Qian, "Design and analysis of the droop control method for parallel inverters considering the impact of the complex impedance on the power sharing," *IEEE Trans. on Ind. Elec.*, vol. 58, no. 2, pp. 576–588, Feb 2011.

[14] M. Savaghebi, A. Jalilian, J. Vasquez, and J. Guerrero, "Secondary control scheme for voltage unbalance compensation in an islanded droop-controlled microgrid," *IEEE Transactions on Smart Grid*, vol. 3, no. 2, pp. 797–807, June 2012.

[15] L. Meng and J. M. Guerrero, "Optimization for customized power quality service in multibus microgrids," *IEEE Transactions on Industrial Electronics*, vol. 64, no. 11, pp. 8767–8777, Nov 2017.

[16] A. García-Cerrada, O. Pinzón-Ardila, V. Feliu-Batlle, P. Roncero-Sánchez, and P. García-Gonzalez, "Application of a repetitive controller for a three-phase active power filter," *IEEE Transactions on Power Electronics*, vol. 22, no. 1, pp. 237–246, 2007.

[17] K. Tammy, "Active control of radial rotor vibrations," Ph.D. dissertation, Helsinki University of Technology (Espoo, Finland), 2007.

[18] D. Chen, J. Zhang, and Z. Qian, "Research on fast transient and $6n\pm1$ harmonics suppressing repetitive control scheme for three-phase grid-connected inverters," *IET Power Elec.*, vol. 6, no. 3, pp. 601–610, 2013.

[19] J. Roldán-Pérez, A. García-Cerrada, J. L. Zamora-Macho, P. Roncero-Sánchez, and E. Acha, "Troubleshooting a digital repetitive controller for a versatile dynamic voltage restorer," *International Journal of Electrical Power & Energy Systems*, vol. 57, no. 0, pp. 105–115, 2014.

[20] G. Escobar, M. Hernandez-Gomez, A. A. Valdez-Fernandez, M. J. Lopez-Sanchez, and G. A. Catzin-Contreras, "Implementation of a $6n\pm1$ repetitive controller subject to fractional delays," *IEEE Transactions on Industrial Electronics*, vol. 62, no. 1, pp. 444–452, Jan 2015.

[21] R. Nazir, K. Zhou, N. Watson, and A. Wood, "Analysis and synthesis of fractional order repetitive control for power converters," *Electric Power Systems Research*, vol. 124, pp. 110–119, 2015.

[22] Z. X. Zou, K. Zhou, Z. Wang, and M. Cheng, "Frequency-adaptive fractional-order repetitive control of shunt active power filters," *IEEE Trans. on Ind. Elec.*, vol. 62, no. 3, pp. 1659–1668, March 2015.

[23] G. Escobar, G. A. Catzin-Contreras, and M. J. Lopez-Sanchez, "Compensation of variable fractional delays in the $6k\pm1$ repetitive controller," *IEEE Transactions on Industrial Electronics*, vol. 62, no. 10, pp. 6448–6456, Oct 2015.

[24] H. Akagi, E. H. Watanabe, and M. Aredes, *Instantaneous Power Theory and Applications to Power Conditioning*. Wiley, 2007.

[25] J. Roldán-Pérez, M. Prodanovic, and A. Rodríguez-Cabero, "Parallel current-controlled synchronverters for voltage and frequency regulation in weak grids," in *9th International Conference on Power Electronics, Machines and Drives*, November 2018.

[26] K. Zhou and D. Wang, "Digital repetitive learning controller for three-phase CVCF PWM inverter," *IEEE Transactions on Industrial Electronics*, vol. 48, pp. 820–830, 2001.

[27] A. Yazdani and R. Iravani, *Voltage-Sourced Converters in Power Systems*. Wiley, 2010.

[28] B. Kuo, *Automatic control system*. Prentice-Hall International London, 1962.